Detection Limit of Gold Nanoparticles in Benchtop K and L Shell X-ray Fluorescence Computed Tomography (XFCT): Monte Carlo Study

Seongmoon Jung, Wonmo Sung, and Sung-Joon Ye*
Biomedical Radiation Sciences, Department of Transdisciplinary Studies
Graduate School of Convergence Science and Technology, Seoul National University, Seoul, Korea
Biomedical Research Institute, Seoul National University College of Medicine, Seoul, Korea
**Corresponding author: sye@snu.ac.kr*

1. Introduction

Among various high-Z nanoparticles, a gold nanoparticles (GNP) has an advantage as follows: It offers not only tumor targeting, drug delivery, and contrast in imaging techniques but also dose enhancement in radiotherapy. In order to determine the *in vivo* concentration and distribution of GNP, detection of X-ray fluorescence (XRF) was proposed [1]. The X-ray fluorescence computed tomography (XFCT) first used a monochromatic synchrotron X-ray source [2]. Recently it has been developed to a benchtop system using polychromatic X-ray sources [1].

A few Monte Carlo (MC) codes such as MCNP5 [3], EGSnrc [4], and Geant4 [5] were utilized to improve the imaging system. Those MC models were validated with experimental measurements [3], [5]. Since MCNP5 offers one L-XRF peak that is an average value of all L-shell fluorescence X-rays, it has only been used for K-XFCT simulations only. MCNP6 includes a new physics data library (i.e., eprdata12) for low-energy photon/electron transport [6].

In this study, the transition probabilities and energies of L-XRF from MCNP6 with eprdata12 were compared with those from other MC codes (PENELOPE and Geant4-GATE). We investigated the detection limits of benchtop polychromatic K- and L-XFCT systems on various phantom sizes using MCNP6.

2. Materials and Methods

2.1 L-shell XRF in Monte Carlo Codes

In order to compare the L shell XRF transition probabilities and X-ray energies, we constructed the simple geometries as shown in figure 1. We used MCNP6, PENELOPE, and GATE Monte Carlo codes to obtain L-XRF emitted from 0.1 wt% GNP inserted in 1-cm-diam. water phantom. MCNP6 and GATE use the Evaluated Atomic Data Library (EADL) which include the transition probabilities and X-ray energies [6], [7]. PENELOLPE uses the same library for the transition probabilities, while the energies of X-rays are taken from the compilation by Deslattes et al [8]. 62 kVp photons were used to irradiate the GNPs. We simulated 10^7 particles for each simulation.

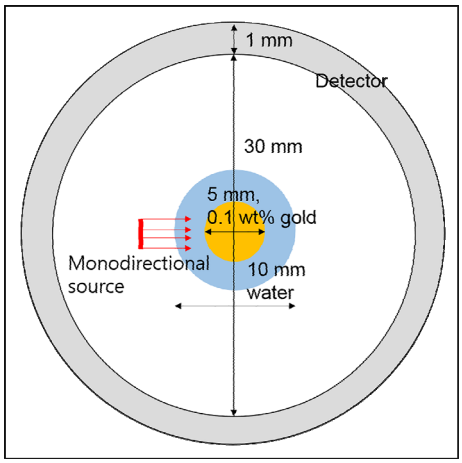

Figure 1. Simulation geometry to compare L-XRF emissions in three MC codes

2.2 Monte Carlo Model for XFCT

The exact dimension and material of the head of detectors were considered in our simulations. For K-shell XFCT, XR-100T CdTe detector (Amptek, USA) was modeled. On the other hands, for L-shell XFCT, XR-100SDD silicon drift detector (Amptek, USA) was constructed as illustrated in figure 2. We defined the GNP which had a 5-mm-diam. and 0.005, 0.01, 0.05, and 0.1 wt% concentrations. The spherical water phantoms were 0.75, 1, 3, and 5 cm diameter. 105 kVp filtered with 0.9 mm tin was used to stimulate K-XRF, while 62 kVp used for detecting L-XRF. The energy spectrum of photons passing through the active area of detectors were obtained by cell flux tally (i.e., F4) and energy bin tally. In order to acquire the true XRF signals, subtracting Compton background was required. The polynomial interpolation fitting to background curve was conducted. 10^{10} particles were simulated for each model.

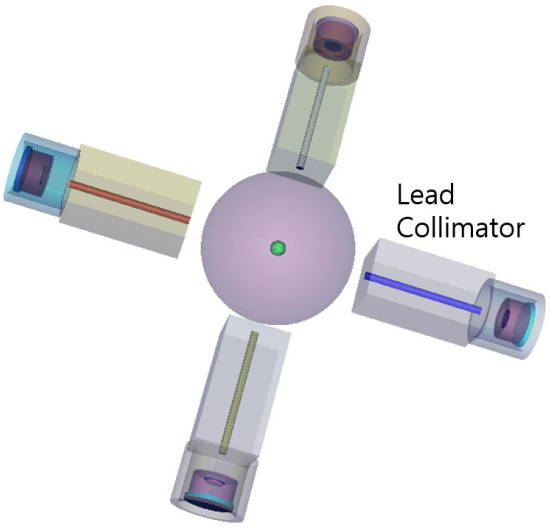

Figure 2. MC model for L shell XFCT

3. Results

3.1 L-shell XRF in Monte Carlo Codes

The energy spectrum from three codes are described in figure 3. MCNP6 with a default physics library emitted only one L-XRF peak. MCNP6 with a new data library showed similar emission rates with PENELOPE (maximum difference within 6%), while it had about 37% higher L_{III}-XRF (i.e., ~9.7 keV) than GATE had. The energies of fluorescence X-rays were different in PENELOPE, because it uses a different data library for X-ray energies [8]

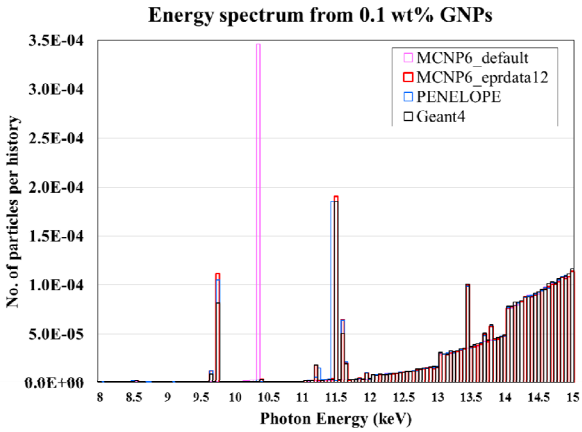

Figure 3. Energy spectra from 0.1 wt% GNPs in 1-cm-diam. water phantom irradiated by 62 kVp photons.

3.2 Net XRF signals

Figure 4 shows net L and K XRF along the concentrations of GNPs. 0.005 wt% GNPs in the 1-cm-diam. phantom could be detected. However, we could not see XRF peaks from even 0.1 wt% GNP in 3-cm-diam. phantom. On the other hand, K-XRF from 0.05 wt% GNPs in 5-cm-diam. phantom was acquired. K-XRF signals from GNPs whose concentrations were below 0.05 wt% GNP were lower than the Compton background uncertainty. Therefore, they should not be considered as XRF signals.

4. Conclusions

We compared the transition probabilities and energies of fluorescence X-rays of MCNP6 implementing a new data library with those of other Monte Carlo codes. MCNP6 showed similar transition probabilities with PENELOPE, while there were some differences in energies of fluorescence X-rays emitted from radiation transition. The number of L_{III} XRF from MCNP6 was about 37% higher than that from GATE. It may be due to a different sampling method used for the transition probabilities. In our simulations, the detection limits were 0.05 wt% and 0.005 wt% in 5-cm-diam. phantom and 1-cm-diam. phantom, respectively. The L shell XFCT provided better sensitivity in shallow depths (i.e., less than 1 cm diameter) than K shell XFCT. However, in order to obtain the distribution of GNP from a small animal larger than 3 cm diameter, the K shell XFCT would be recommended.

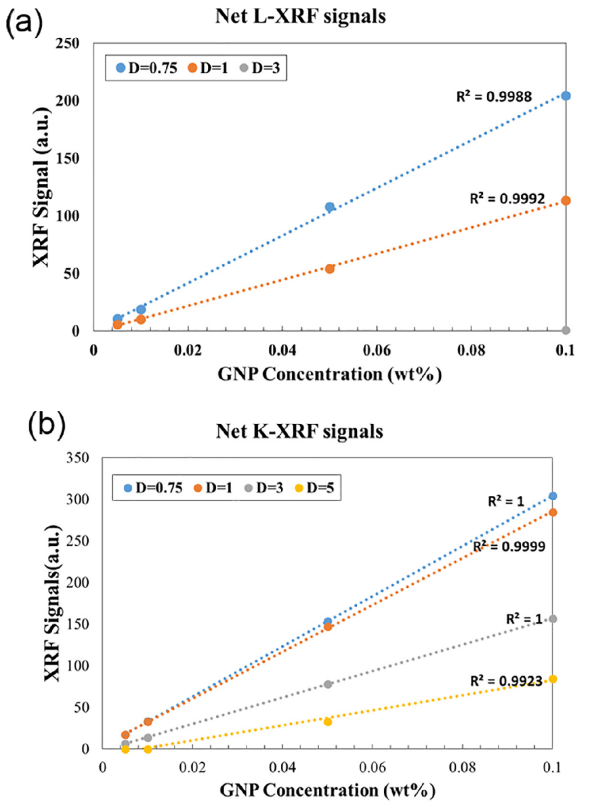

Figure 4. Net XRF signals acquired by MCNP6 simulations. (a) L-XRF signals vs. GNP concentrations. (b) K-XRF signals vs. GNP concentrations. D in the legends indicates the diameter of water phantom in cm.

REFERENCES

[1] B. L. Jones, N. Manohar, F. Reynoso, A. Karellas, and S. H. Cho, "Experimental demonstration of benchtop X-ray fluorescence computed tomography (XFCT) of gold nanoparticle-loaded objects using lead- and tin-filtered polychromatic cone-beams," *Phys Med Biol,* vol. 57, pp. N457-67, Dec 7 2012.
[2] P. Boisseau, "Determination of three dimensional trace element distributions by the use of monochromatic X-ray microbeams," Ph.D. dissertation, Dept. Phys., Massachusetts Inst. Technol., Cambridge, MA, 1986.
[3] N. Manohar, B. L. Jones, and S. H. Cho, "Improving X-ray fluorescence signal for benchtop polychromatic cone-beam X-ray fluorescence computed tomography by incident X-ray spectrum optimization: a Monte Carlo study," *Med Phys,* vol. 41, p. 101906, Oct 2014.
[4] M. Ahmad, M. Bazalova, L. Xiang, and L. Xing, "Order of magnitude sensitivity increase in X-ray Fluorescence Computed Tomography (XFCT) imaging with an optimized spectro-spatial detector configuration: theory and simulation," *IEEE Trans Med Imaging,* vol. 33, pp. 1119-28, May 2014.
[5] M. Bazalova-Carter, M. Ahmad, T. Matsuura, S. Takao, Y. Matsuo, R. Fahrig*, et al.*, "Proton-induced x-ray fluorescence CT imaging," *Med Phys,* vol. 42, pp. 900-7, Feb 2015.
[6] H. G. Hughes, Enhanced Electron-Photon Transport in MCNP6, LA-UR-13-27632, 2013.
[7] S. Guatelli, A. Mantero, B. Mascialino, P. Nieminen, and M. G. Pia, "Geant4 Atomic Relaxation", IEEE Trans. Nucl. Sci. vol.54, no.3., 2007.
[8] F. Salvat, J. M. Fernndez-Varena and J. Sampau, "Penelope-2011 A code system for Monte Carlo simulation of electron and phonon transport" OECD, 2011.